Article │ Received 26 February 2025; Accepted 27 April 2025; Published 16 May 2025
https://doi.org/10.55092/sc20250012

# Assessing the low-carbon potential of magnesium silicate hydrate cement: a probabilistic life cycle approach

**Yue Li[1,2], Xiao Luo[1,2,*], Xiaolong Liu[1], Zhijie Zhang[1], Kun Meng[1] and Jinlei Mu[3]**

[1] Key Laboratory of Urban Security and Disaster Engineering of Ministry of Education, Beijing Key Laboratory of Earthquake Engineering and Structural Retrofit, Beijing University of Technology, Beijing 100124, China
[2] Chongqing Research Institute of Beijing University of Technology, Chongqing 401121, China
[3] Hebei Institute of Architecture Civil Engineering, Hebei University of Architecture, Zhangjiakou 075132, China

* Correspondence author; E-mail: luoxiao@emails.bjut.edu.cn.

## Highlights:

- Analysis shows MSHC is not definitively low-carbon, with emissions tied to mix proportions.
- The amounts of L-MgO and siliceous raw materials are key factors influencing carbon emissions.
- L-MgO is the primary factor contributing to the uncertainty in MSHC carbon emissions.
- Using machine learning, a low-carbon MSHC mix is identified when the Mg/Si is below 0.8.

**Abstract:** Magnesium silicate hydrate cement (MSHC), as an innovative low-carbon cementitious material, is considered a potential substitute for ordinary Portland cement (OPC). However, uncertainties in the carbon emission factors of raw materials and mix proportions pose challenges for assessing its life cycle carbon emissions. This study employs a probabilistic life cycle assessment (PLCA) to evaluate the carbon emission intensity of MSHC and analyze its uncertainties. Leveraging machine learning techniques, a predictive model for the carbon emission intensity of MSHC was developed, and sensitivity analysis was conducted on various characteristic parameters. The results indicate that although MSHC is regarded as a low-carbon material, it does not exhibit low-carbon characteristics in all scenarios compared to OPC. The carbon emission intensity of MSHC is closely related to its mix proportions. Depending on different mix proportions, the average carbon emissions of MSHC range from 0.174 to 1.419 kg CO2e/kg. L-MgO is a key factor influencing the uncertainty of MSHC carbon emissions. Notably, the Mg/Si ratio is a critical factor influencing the carbon emission characteristics of MSHC, with a low-carbon threshold range observed between approximately 0.8 and 1.0.

**Keywords:** magnesium silicate hydrate cement; carbon emissions; probabilistic life cycle assessment; uncertainty analysis; machine learning

## 1. Introduction

As the issue of global warming becomes increasingly acute, sustainable development has become a pivotal focus within the construction industry. Cement, as a foundational material in this sector, has an environmental impact during production that cannot be ignored. It is estimated that the $CO_2$ emissions of the cement industry account for 7%–8% of the global total carbon emissions [1]. Ordinary Portland Cement (OPC), the most commonly used cementitious material, has relatively high carbon emissions [2]. Data indicates that the production of one ton of OPC results in 0.73–0.99 tons of carbon emissions [3]. Consequently, the development of new low-carbon cementitious materials has become a focus of research among scholars.

Magnesium silicate hydrate cement (MSHC) is a novel green cementitious material considered a potential alternative to OPC. It is typically prepared by mixing lightly calcined magnesium oxide (L-MgO), siliceous raw materials (SRM), water-reducing agents (WRA), and water [4]. MSHC possesses many outstanding properties, such as low pH, light weight, high strength, excellent heat resistance, and corrosion resistance [5,6]. These characteristics confer MSHC with significant potential in applications such as management of low to intermediate-level radioactive waste and the production of insulation panels [4,7].

In addition, compared to OPC, MSHC is considered to have advantages in terms of low carbon emissions. This is because the calcination temperature of lightly calcined MgO ranges between 700–1000 °C [8], which is significantly lower than that required for OPC. This lower calcination temperature translates to reduced energy consumption and carbon emissions during production. Additionally, MSHC typically utilizes industrial by-products such as silica fume and fly ash, further contributing to carbon emission reduction. However, despite numerous studies highlighting the low-carbon characteristics of MSHC [9–11], quantitative research on the entire life cycle carbon emissions of MSHC remains limited. Therefore, further quantitative validation is necessary to establish scientific evidence on whether MSHC can be considered a low-carbon cementitious material.

Life cycle assessment (LCA) method is used to identify and quantify the environmental impacts of products throughout their entire life cycle. This approach has been widely applied in cement production [12]. However, traditional cement LCA tools have certain limitations in their use. It relies too heavily on specific sample data and fails to comprehensively consider issues such as data uncertainty due to regional differences, production conditions, and product mix characteristics. This results in lower applicability and reference value in practical applications [13]. In the carbon emission assessment of MSHC, the limitations of conventional LCA methods become particularly pronounced. Specifically, the diversity in raw material types, production processes, and treatment methods leads to significant variations in the carbon emissions associated with different materials. For instance, the carbon emissions of L-MgO are influenced by multiple factors, including calcination temperature and the type of energy source used. Similarly, the carbon footprint of water-reducing agents, such as polycarboxylate ether and sodium hexametaphosphate, varies depending on their respective production processes. Furthermore, SRM-including silica fume, fly ash, blast furnace slag, and metakaolin-exhibit distinct carbon emission profiles due to differences in their processing and recycling methods. Additionally, adjustments in material ratios (such as the L-MgO-to-SRM ratio) can significantly alter the carbon intensity of MSHC. Taken together, the variability in production techniques, treatment procedures, and mix designs results in considerable uncertainty in the carbon emissions of MSHC. Therefore, it is necessary to develop a more flexible LCA

method. This method can utilize the extensive existing research results to more accurately simulate and predict the carbon emission intensity of MSHC, thereby enhancing its applicability. Studies have shown that a probabilistic life cycle assessment (PLCA) approach can adequately account for data uncertainty. This method changes a solitary carbon emission figure into a range or probabilistic distribution, offering a more precise and unbiased representation of the true carbon emissions[14]. In this way, the PLCA method can not only better address the complex production conditions of MSHC raw materials but also provide more reliable information for decision-makers.

Furthermore, with the continuous advancement of data-driven technologies, an increasing number of studies have begun to utilize machine learning (ML) techniques to predict and optimize the performance and carbon emission characteristics of construction materials. For instance, Xing *et al.* developed a multilayer perceptron model using ML to predict the carbon emissions and energy consumption of cement based on 570 concrete mix design datasets containing recycled aggregates and supplementary cementitious materials [15]. Amin Al-Fakih *et al.* employed AI technologies, including ML models and stacked ensemble methods, to predict the carbon footprint of ground granulated blast furnace slag geopolymer concrete [16]. Similarly, Wang *et al.* proposed a method combining ML with a multi-objective optimization model to optimize the proportions of geopolymer mixtures. This method enhances compressive strength while minimizing carbon emissions and costs, providing a new approach for the multi-objective optimization design of low-carbon cement [17]. P.S.M. Thilakarathna *et al.* used ML algorithms to analyze the embodied carbon emissions of high-strength concrete, calculating the carbon footprint of different mix components and offering guidelines for producing low-carbon high-strength concrete [18]. These studies demonstrate the significant potential of ML techniques in the research of low-carbon cement-based materials. By utilizing ML models, it is possible to more accurately predict the impact of different materials and processes on carbon emissions, thereby optimizing mix designs and production processes to promote the development of low-carbon materials.

In conclusion, this study employs a PLCA method to conduct a quantitative evaluation and uncertainty analysis of the carbon emissions of MSHC, with the aim of filling a research gap in this field. First, the research objectives and system boundaries of the LCA were defined. Extensive data on carbon emission factors from raw materials and transportation processes were collected, and their optimal distribution models were established. Subsequently, the Monte Carlo method was employed to conduct a quantitative assessment of the carbon emission intensity for 13 different MSHC mix ratios. an uncertainty analysis of the carbon emissions of each component was performed. Building on this foundation, ML techniques were employed to develop a predictive model for carbon emission of MSHC, accompanied by feature importance analysis. Furthermore, leveraging the PLCA method and a ML model, two graphical user interfaces (GUI) were created to facilitate swift analysis and evaluation of MSHC carbon emissions. The technical roadmap of this study was depicted in Figure 1.

The innovations of this study are as follows: (1) The adoption of the PLCA method to systematically and quantitatively evaluate the carbon emissions of MSHC, providing a detailed data foundation and scientific methodology. (2) Through uncertainty analysis, the study reveals the contributions and variation ranges of different parts in MSHC's carbon emissions, identifying the main sources of uncertainty. (3) The introduction of ML technology has led to the development of a carbon emission prediction model for MSHC, making carbon emission predictions more intelligent and accurate. Further feature importance analysis identified the key factors, providing strong support for formulating effective

carbon reduction strategies. This study provides a solid foundation for the in-depth understanding and optimization of MSHC's carbon emissions. Additionally, it contributes to the development of more targeted and scientific carbon reduction measures, thereby promoting the sustainable development of the building materials industry and the achievement of environmental protection goals.

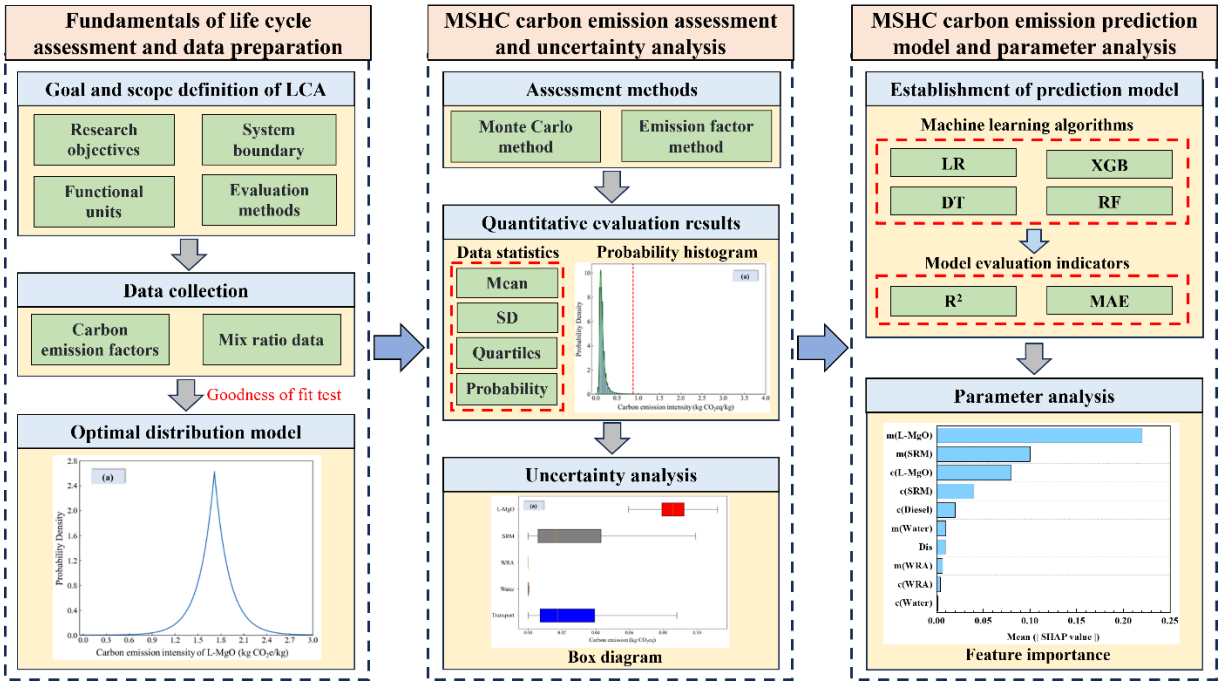


**Figure 1.** General roadmap.

## 2. Methodology

Sufficient details of the experiment, methods, simulation, calculation, statistical test or analysis should be given so that the method could be repeated by another researcher and the results reproduced. Note and emphasize any hazards such as explosive or toxicity, better with a separate section by the heading "Caution". In theoretical papers, this section can be called "Theoretical Basis" or "Theoretical Calculations".

### *2.1. Goal and scope definition of LCA*

This research utilized a PLCA approach to examine both the direct and indirect carbon emissions of MSHC across its life cycle, spanning from raw material acquisition and transportation to production (cradle-to-gate). By calculating the $CO_2$ equivalents released per kilogram of MSHC produced, the overall carbon emissions were assessed. A comparison with the carbon emissions of OPC was conducted to evaluate whether MSHC possesses low-carbon characteristics. MSHC is prepared by mixing a specific ratio of lightly burned magnesium oxide, siliceous raw materials, water reducer, and water. In this system, MgO dissolves in water and ionizes into $Mg^{2+}$ (Equation 1). In an alkaline environment, $SiO_2$ dissolves to form $H_2SiO_4^{2-}$ and $H_3SiO_4^{-}$ (Equation 2). Ultimately, $Mg^{2+}$ reacts with $H_2SiO_4^{2-}$ and $H_3SiO_4^{-}$ to form M-S-H gel (Equation 3), which is key to its strength support. This reaction can typically occur at room temperature [19]. Therefore, the carbon emissions during the production and processing stages of MSHC were ignored. The specific system boundary was illustrated in Figure 2.

$$MgO + H_2O \rightarrow Mg^{2+} + 2OH^- \leftrightarrow Mg(OH)_2 \quad (1)$$

$$SiO_2 + 2OH^- \rightarrow H_2SiO_4^{2-}$$
$$SiO_2 + 2OH^- + H_2O \rightarrow H_3SiO_4^- \quad (2)$$

$$3Mg^{2+} + 4OH^- + 2H_3SiO_4^- \leftrightarrow 3MgO \cdot 2SiO_2 \cdot 2H_2O + 3H_2O$$
$$3Mg^{2+} + 2OH^- + 4H_3SiO_4^- \leftrightarrow 3MgO \cdot 4SiO_2 \cdot H_2O + 6H_2O$$
$$3Mg^{2+} + 2OH^- + 2H_2SiO_4^{2-} \leftrightarrow 3MgO \cdot 2SiO_2 \cdot 2H_2O + H_2O \quad (3)$$
$$3Mg^{2+} + 4H_2SiO_4^{2-} \leftrightarrow 3MgO \cdot 4SiO_2 \cdot H_2O + 2OH^- + 2H_2O$$

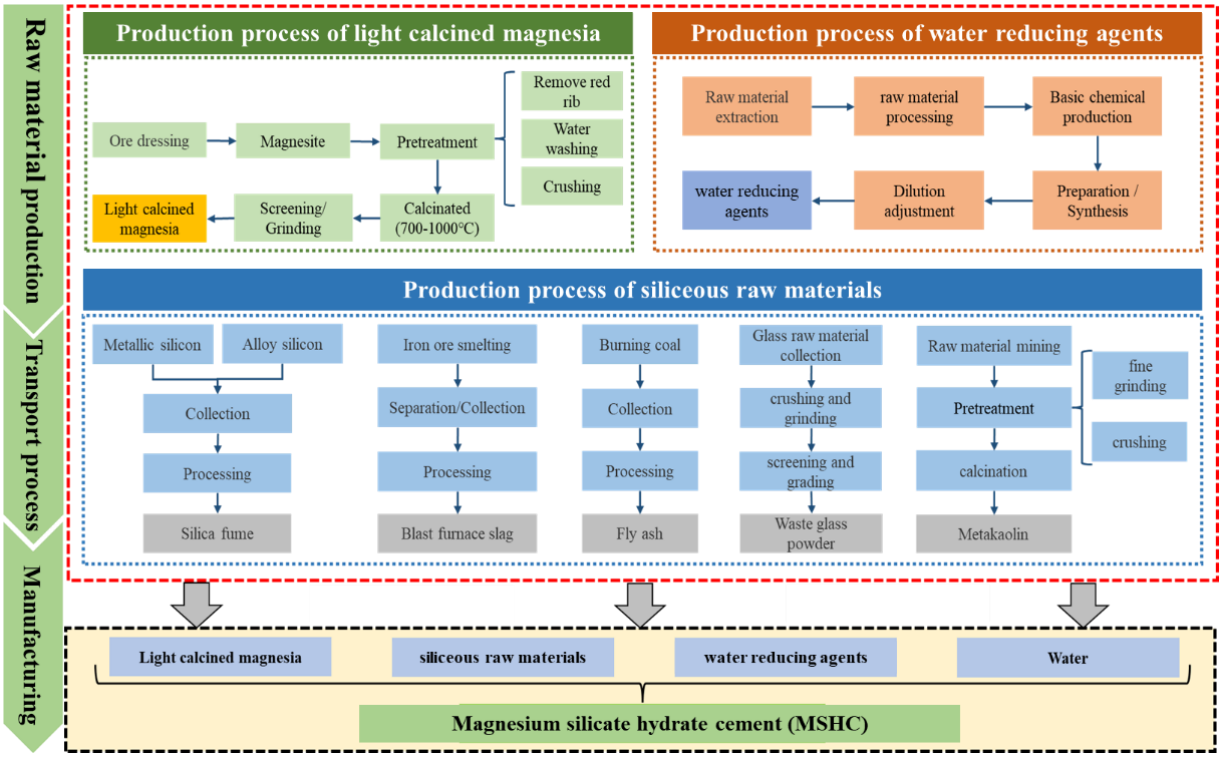


**Figure 2.** System boundary.

Through the analysis of the production and transportation processes of various components of MSHC, the main sources of its carbon emissions were identified as follows:

(1) Production of L-MgO: L-MgO was primarily derived from magnesium-rich ores such as magnesite and dolomite. The extraction process of these ores consumed energy, resulting in the release of carbon dioxide. Throughout the manufacturing process of L-MgO, the magnesium ores underwent calcination at temperatures between 700 °C and 1000 °C, generating both direct and indirect carbon emissions. Direct carbon emissions originated from the decomposition of magnesium ores (as shown in Equation 4) and the combustion of fuels. Indirect carbon emissions mainly stemmed from the production of fuels and electricity. Additionally, subsequent processing steps such as grinding and molding of L-MgO also required energy consumption, leading to further carbon emissions.

$$MgCO_3 \rightarrow MgO + CO_2 \uparrow \quad (4)$$

(2) Processing of SRM: The carbon emissions of SRM primarily involved the consumption of fossil fuels during industrial mining and processing, as well as the energy consumption of mechanical equipment in the waste collection process. Additionally, the post-processing stages (such as heat treatment and grinding) also required energy, further increasing carbon emissions.

(3) Production of WRA: The production process of WRA involved heating, mixing, and dispersing, which typically required the consumption of electricity or other fossil fuels such as natural gas and oil. The combustion of these fuels directly released $CO_2$. Additionally, the key components of WRA included various chemical raw materials. The production of these chemicals required the processing of raw materials and complex chemical synthesis. These steps all involved energy consumption, thereby leading to increased carbon emissions.

(4) Water supply process: The stages of water extraction, purification, and distribution all required energy consumption. This was typically directly associated with carbon emissions. For instance, the electric power for pumping equipment, the electricity and chemical agents used in water treatment processes, as well as the operation of water pumps and the distribution network, all demanded substantial amounts of electricity, thereby resulting in carbon emissions.

(5) Transport process: This study assumed that the transportation of raw materials was carried out using diesel-powered freight trucks. Due to geographical differences in various regions, the transportation distances of raw materials could vary. According to relevant literature, most raw materials were typically transported over distances ranging from 10 to 250 kilometers [14]. The combustion of diesel fuel during transportation led to carbon emissions.

In summary, the carbon emissions of MSHC throughout its life cycle-from raw material acquisition to final product manufacturing-primarily included ore decomposition, energy consumption (such as electricity and fuel), chemical processes, and transportation.

### *2.2. Life cycle inventory analysis*

Central to the LCA analysis was the life cycle inventory (LCI). Based on the established boundaries of the LCA system, data required for the PLCA carbon emissions analysis of MSHC were collected and processed.

#### 2.2.1. Data collection

The data used for calculating MSHC carbon emissions primarily includes two categories: first, the carbon emission factors of various raw materials and their transportation processes, and second, the mixing ratios of MSHC. Due to differences in production conditions (such as energy types, consumption levels, production efficiency, and equipment usage), the carbon emission factors of raw materials vary significantly across different time periods and countries. Furthermore, varying transportation distances and vehicle efficiencies are also important influencing factors. These elements contribute to the uncertainty of carbon emission factors. It is crucial to carefully consider these uncertainties during the life cycle assessment as they directly impact the final environmental impact evaluation results.Therefore, we have extensively collected data from multiple countries and regions worldwide, spanning from 2005 to 2024, with most data concentrated around the year 2020. This highlights the timeliness and relevance of our research. The specific statistical results of the data were shown in Table 1. Literature sources for carbon emission factors: L-MgO [20–23], SRM [24-27], WRA [28-31], Water [32-34], Diesel [14,23,35].

**Table 1.** Carbon emission factor statistics (Units: kg $CO_2$e/kg, Diesel: kg $CO_2$e/t·km).

| | n | Min | Max | Ave | σ | Skew | Kurt |
|---|---|---|---|---|---|---|---|
| L-MgO | 28 | 1.060 | 2.700 | 1.7075 | 0.2922 | 0.9061 | 4.652 |
| SRM | 70 | 0.0003 | 0.600 | 0.05611 | 0.1075 | 3.1997 | 11.116 |
| WRA | 47 | 0.2500 | 2.388 | 1.4187 | 0.5150 | −0.3638 | −0.251 |
| Water | 25 | 0.000008 | 0.010 | 0.000808 | 0.00197 | 4.6087 | 22.151 |
| Diesel | 15 | 0.018 | 0.918 | 0.2324 | 0.2321 | 2.2918 | 5.425 |

Note: n represents the sample size. Min denotes the minimum value. Max denotes the maximum value. Ave represents the average value. σ denotes the standard deviation. Skew represents skewness, and Kurt denotes kurtosis.

Table 1 revealed the range and characteristics of carbon emission factors for various raw materials and diesel. For instance, the carbon emission factor of L-MgO mainly ranged from 1.06 to 2.7 kg $CO_2$e/kg, with an average value of 1.7075 kg $CO_2$e/kg, indicating a relatively high level of carbon emissions. This was primarily attributed to the extensive use of fossil fuels in the production process of L-MgO and the release of $CO_2$ during the decomposition of magnesium ore. The carbon emission factors for SRM range from 0.0003 to 0.6 kg $CO_2$e/kg, which were relatively lower compared to L-MgO. This indicated that SRM primarily originates from the collection of high-silica industrial wastes, such as silica fume and fly ash. The carbon emission factor for WRA ranged from 0.25 to 2.388 kg $CO_2$e/kg. This significant variation was due to the diversity in WRA production processes and raw material selection. The carbon emission factor for water was generally low, with an average value of 0.000808 kg $CO_2$e/kg. The carbon emission factor for diesel ranged from 0.018 to 0.918 kg $CO_2$e/t·km, with the variation mainly influenced by transportation efficiency. Additionally, by analyzing the kurtosis and skewness of the carbon emission factors for various materials and diesel, it was evident that these data exhibited right-skewed or left-skewed distributions and varying degrees of sharpness. In summary, these observations revealed the uncertainty and complexity of carbon emissions associated with the raw materials of MSHC and their transportation processes.

Regarding the mix proportion, the performance of MSHC was influenced by three key parameters: the magnesium-to-silicon ratio (Mg/Si), the water-to-cement ratio (w/c), and the amount of water-reducing agent (WAR%). The determination of these parameters depended on the type of raw materials and the specific performance requirements that the final product needed to meet.

When the L-MgO content was low (with an Mg/Si ratio ranging from approximately 0.0526 to 0.429), L-MgO primarily acted as an alkaline activator in the reaction system, similar to alkali-activated systems. When the Mg/Si ratio was between 0.533 and 4.0, the system underwent MgO-$SiO_2$ reactions. Within this range, Mg/Si influenced workability, mechanical properties, and volume stability differently. For workability, increasing the Mg/Si ratio enhanced the flowability of MSHC [36]. Regarding mechanical properties, the optimal Mg/Si ratio typically lay between 0.667 and 1.50. Insufficient L-MgO resulted in lower M-S-H gel formation, while excess L-MgO led to the formation of surplus $Mg(OH)_2$, whose expansive nature could reduce the mechanical performance of MSHC [37]. Additionally, a higher Mg/Si ratio could decrease shrinkage due to the expansive properties of $Mg(OH)_2$. Consequently, researchers adjusted the Mg/Si ratio according to specific application requirements.

Due to the lattice structure of L-MgO and the fine particle size of SRM, the water demand of MSHC was usually high [38]. Therefore, an appropriate amount of WRA was added to improve its workability.

Sodium hexametaphosphate (SHMP) was an effective WRA suitable for MSHC. Adding 1% SHMP could reduce the w/c ratio of the system to 0.4 [39]. Additionally, studies showed that adding 1.0%–1.5% polycarboxylate superplasticizer could also significantly reduce the water demand of the system [6].

To comprehensively explain the impact of mix proportions on the carbon emissions of MSHC, this study collected 13 sets of MSHC mix proportions from relevant literature sources [39–43], as shown in Table 2. Given that L-MgO and siliceous raw materials are the primary reactants in MSHC, their proportions significantly influence the final performance and carbon emissions. Therefore, we selected a broad range of Mg/Si ratios to ensure that the study results are widely applicable and representative. Furthermore, these 13 mix proportions are highly cited and recognized in existing research and possess a certain level of engineering practicality. In summary, the selection of these mix proportions aims to ensure the comprehensiveness, representativeness, and operability of the research. The specific data ranges are as follows: the Mg/Si ratio ranges from 0.053 to 4.0, the WAR (%) ranges from 0% to 3.4%, and the w/c ratio ranges from 0.32 to 0.60.

**Table 2.** Mix proportion of MSHC.

| Number | Mg/Si | WAR (%) | w/c |
|---|---|---|---|
| 1 | 0.053 | 0 | 0.32 |
| 2 | 0.111 | 0 | 0.40 |
| 3 | 0.250 | 0 | 0.32 |
| 4 | 0.429 | 0 | 0.50 |
| 5 | 0.533 | 3.4 | 0.45 |
| 6 | 0.667 | 1.0 | 0.40 |
| 7 | 0.800 | 3.4 | 0.41 |
| 8 | 1.000 | 1.0 | 0.55 |
| 9 | 1.333 | 0 | 0.53 |
| 10 | 1.500 | 3.0 | 0.40 |
| 11 | 2.000 | 0 | 0.53 |
| 12 | 2.333 | 4.0 | 0.60 |
| 13 | 4.000 | 2.0 | 0.50 |

### 2.2.2. Parameter uncertainty modeling

To address the aforementioned uncertainty in carbon emission factors and to more accurately describe the distribution characteristics of these factors, the collected data was analyzed using goodness-of-fit and parameter estimation methods [44]. In this process, firstly, the Kolmogorov-Smirnov statistics and corresponding p-values of 19 distribution types (t Location-Scale distribution, Beta distribution, Chi-square distribution, Exponential distribution, F distribution, Gamma distribution, Weibull distribution, Laplace distribution, Generalized Extreme Value distribution, Maximum extreme value distribution, Minimum extreme value distribution, Stable distribution, Burr distribution, Nakagami distribution, Logistic distribution, Log-normal distribution, Normal distribution, Triangular distribution, Uniform distribution) were compared. This step aimed to preliminarily determine whether the data conformed to a specific distribution pattern and to screen out candidate distribution models that closely matched the data distribution. Secondly, to further

determine the optimal distribution model, the Akaike Information Criterion (AIC, Equation 5) and the Bayesian Information Criterion (BIC, Equation 6) were introduced. In these equations, k represents the number of parameters in the model, L is the maximum likelihood estimate of the model, and n denotes the number of data points. AIC and BIC aided in selecting the best statistical model, mainly used to evaluate the model fitting quality. When comparing multiple models, the model with the minimum AIC and BIC values was usually considered the optimal one.

$$AIC = 2k - 2\ln(L) \tag{5}$$

$$BIC = k\ln(n) - 2\ln(L) \tag{6}$$

*2.3. Carbon emission intensity simulation*

To thoroughly evaluate the carbon emissions of MSHC and address the uncertainty in the carbon emission factors, several steps were implemented. Initially, utilizing the Monte Carlo method, one million random samples were drawn for the previously mentioned carbon emission factors and transportation distances. Then, using the emission factor method (Equation 7) [45], the estimated carbon emissions for one million instances of MSHC for each mix proportion were calculated. Finally, an in-depth analysis of the MSHC carbon emissions was conducted, including statistical characteristic analysis and visualization of the data. These analytical results comprehensively reflected the quantitative characteristics of MSHC carbon emissions and provided reliable data support for carbon emission of MSHC.

$$E_i = AD_i \times EF_i \tag{7}$$

In the Equation 4, i denotes the component i in MSHC. $E_i$ represents the greenhouse gas ($CO_2$) emissions resulting from the consumption or energy use of component i. $AD_i$ indicates the activity data (or usage) of the consumption or energy use of component i. $EF_i$ denotes the carbon emission factor of component i.

*2.4. Carbon emission prediction analysis*

In this study, the mix proportion data for 13 types of MSHC were collected. However, this did not cover all possible scenarios. To address this issue, we employed a machine learning model to predict the carbon emission across a wider range of MSHC mixing ratios. To gain deeper insights into the relationship between various feature parameters and the carbon emission intensity of MSHC, Shapley Additive Explanations (SHAP) were also applied.

2.4.1. ML model establishment and performance evaluation

In this study, we employed four ML algorithms from the sklearn Python library: Linear Regression (LR), Decision Tree (DT), Random Forest (RF), and Extreme Gradient Boosting (XGB). Each algorithm has distinct principles and attributes, making them appropriate for various types of problems and datasets. Detailed principles and characteristics of each algorithm can be found in relevant literature [46].

The prediction performance of the machine learning models was evaluated using metrics such as the coefficient of determination (*i.e.*, $R^2$, as shown in Equation 8) and Mean Absolute Error (*i.e.*, MAE,

as shown in Equation 9). Among these metrics, $R^2$ was primarily employed to assess how well the model fit the actual data. MAE was utilized to assess the prediction errors of the models.

$$R^2 = 1 - \frac{\sum_{i=1}^{N}(y_i - y_i')^2}{\sum_{i=1}^{N}(y_i - \bar{y})^2} \quad (8)$$

$$MAE = \frac{1}{N}\sum_{i=1}^{N}|y_i - y_i'| \quad (9)$$

In these formulas, y and ȳ represented the actual values and their mean, respectively, while y' and ȳ' represented the predicted values and their mean, respectively. N denoted the sample size.

2.4.2. SHAP analysis

SHAP analysis is a method for interpreting the output of ML models, based on the concept of Shapley values. Shapley values originate from cooperative game theory and are used to fairly distribute collaborative gains. In ML, SHAP analysis explains model outputs by calculating the contribution of each feature to the prediction results. By aggregating the SHAP values of all samples, it is possible to understand which features are most important to the model's predictions overall. This quantifies the impact of input variables on the model's predictions and helps researchers understand the mechanisms of MSHC carbon emissions.

## 3 Results and discussion

### *3.1. Parameter uncertainty modeling results*

By using the goodness-of-fit testing methods described in Section 2.2.1, the optimal probability distribution models for the carbon emission factors of various components were determined. The probability distribution plots were shown in Figure 3, and the distribution types and parameters were listed in Table 3.

**Table 3.** Statistical parameters for the optimal probability distribution of the carbon emission factors.

| | Distribution type | Distribution parameters | p value | AIC | BIC |
|---|---|---|---|---|---|
| L-MgO | Laplace distribution | μ = 1.716; b = 0.190 | 0.997 | 5.89 | 8.54 |
| SRM | Burr distribution | c = 1.175; k = 0.819; α = 0.022 | 0.369 | −298.18 | −289.18 |
| WRA | Normal distribution | μ = 1.419; σ = 0.510 | 0.497 | 75.13 | 78.83 |
| Water | Generalized extremum distribution | k = −0.936; μ = 0.0002; σ = 0.000228 | 0.352 | −318.08 | −314.43 |
| Diesel | Chi square distribution | df = 1.944; μ = 1.419; σ = 0.510 | 0.688 | −12.06 | −9.94 |

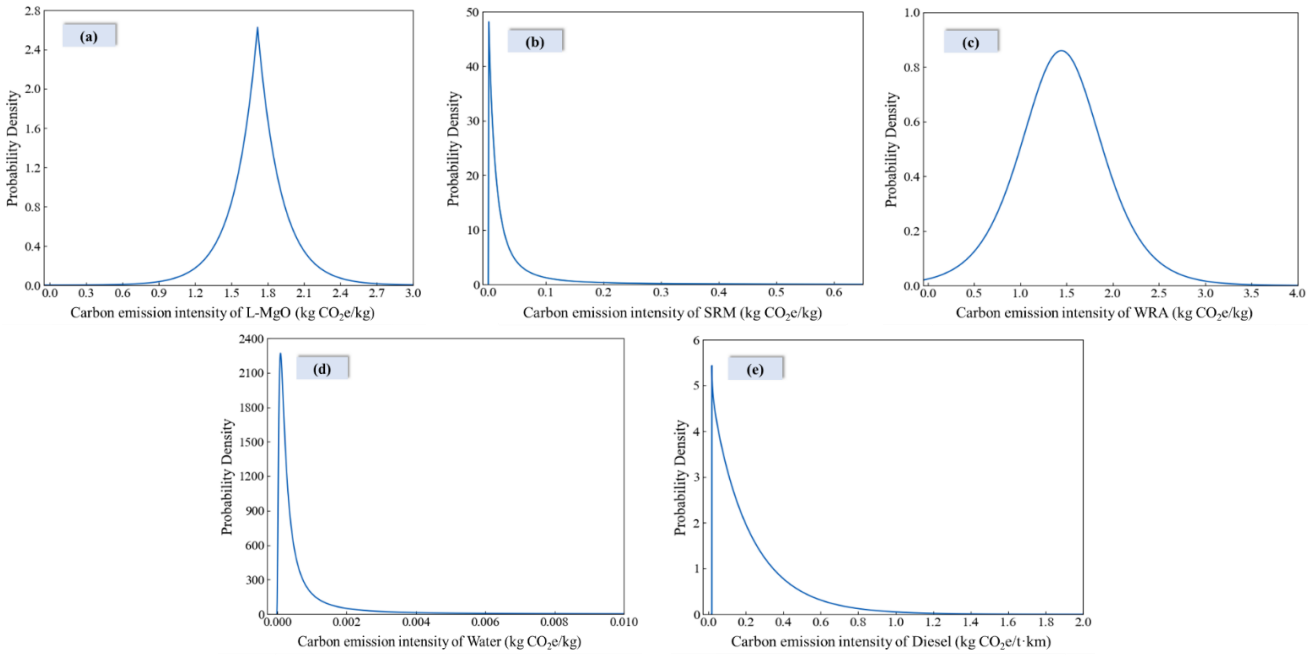


**Figure 3.** Fitted distribution of carbon emission factors.

### *3.2. Analysis of simulation results for carbon emission intensity*

#### 3.2.1. Carbon emission assessment and comparison of MSHC

In this study, the Monte Carlo method was utilized to simulate the carbon emission for MSHC, producing one million simulated values for each mix ratio. The objective was to uncover the carbon emission patterns of MSHC using extensive data results. Figure 4 showed the corresponding histograms and probability density curves (Figure 4(a)–(m) corresponded to the calculation results of mixing ratios 1–13, respectively). In the analysis results, extreme outliers were excluded, and only data with carbon emission intensity between 0 and 4 were included. This filtering ensured the reliability and accuracy of the research data. The statistical outcomes of the carbon emissions data were summarized in Table 4 and Figure 5.

Furthermore, to further investigate the low-carbon characteristics of MSHC in building materials, this study compared the carbon emissions of MSHC with those of OPC, which is widely used in construction. Research indicates that the carbon emission intensity of OPC ranges from 0.811 to 0.977 kg $CO_2$e/kg [8,22]. For a clearer comparison, a reference value of 0.877 kg $CO_2$e/kg was adopted [47], as indicated by the red dashed line in Figure 4 and Figure 5. In the subsequent analysis, we defined mixing ratios with carbon emission intensities lower than that of OPC (0.877 kg $CO_2$e/kg) as “low-carbon”, whereas those with higher carbon emission intensities were defined as “high-carbon”.

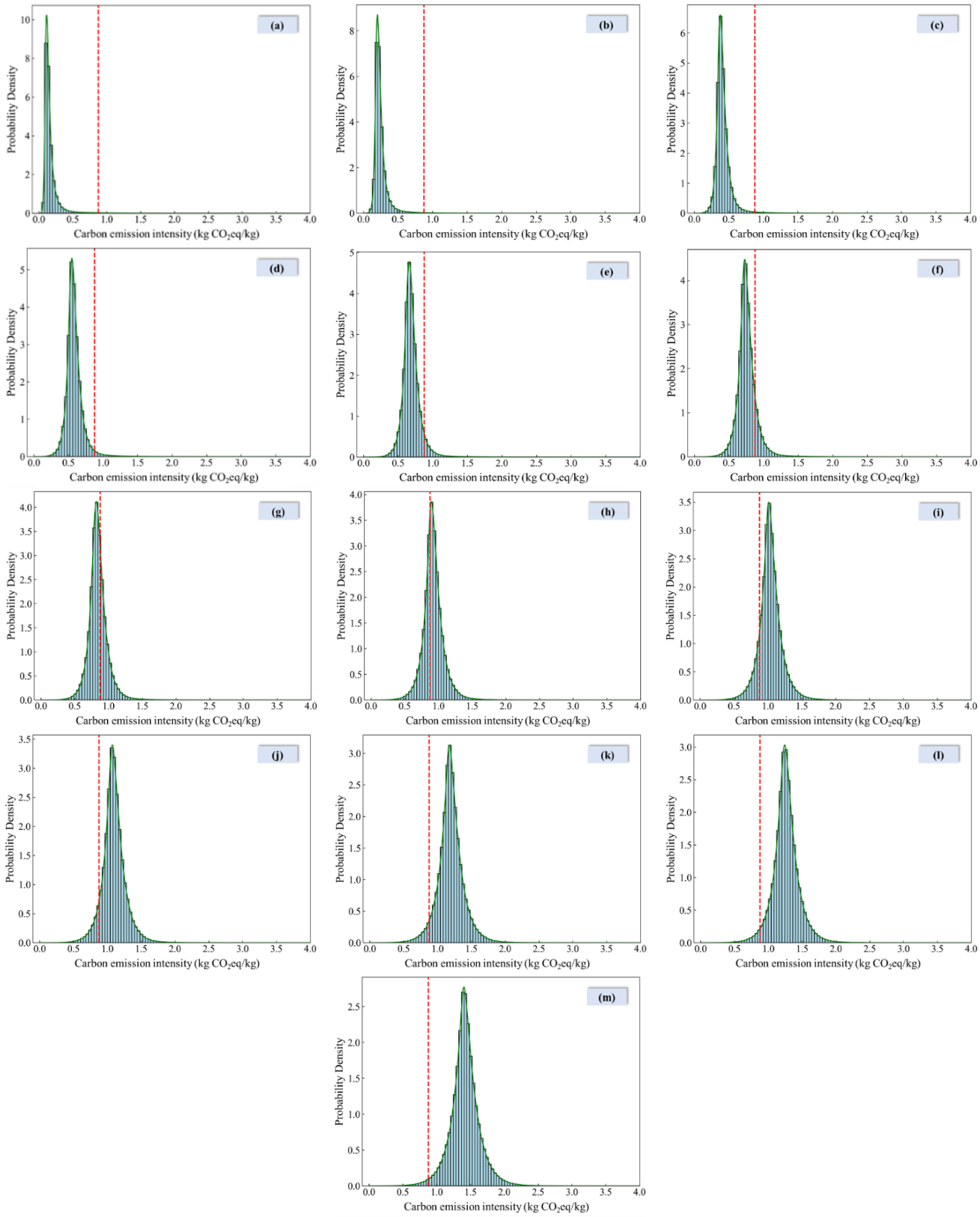


**Figure 4.** For MSHC under different mix ratios, a probability density plot of carbon emission intensity.

**Table 4.** Statistical results of Monte Carlo simulation on carbon emission intensity of MSHC (Unit: kg $CO_2$e/kg).

| Number | Mean | SD | Q1 | Q2 | Q3 | <OPC (%) | Compared to OPC (%) |
|---|---|---|---|---|---|---|---|
| 1 | 0.174 | 0.186 | 0.110 | 0.134 | 0.178 | 98.98 | 80.16 |
| 2 | 0.257 | 0.181 | 0.193 | 0.222 | 0.266 | 98.88 | 70.70 |
| 3 | 0.423 | 0.174 | 0.357 | 0.395 | 0.448 | 98.55 | 51.77 |
| 4 | 0.590 | 0.171 | 0.519 | 0.567 | 0.630 | 97.38 | 32.73 |
| 5 | 0.694 | 0.167 | 0.620 | 0.675 | 0.742 | 93.94 | 20.87 |
| 6 | 0.762 | 0.172 | 0.685 | 0.744 | 0.817 | 86.40 | 13.11 |
| 7 | 0.849 | 0.172 | 0.769 | 0.834 | 0.910 | 66.00 | 3.19 |
| 8 | 0.926 | 0.180 | 0.842 | 0.912 | 0.995 | 36.60 | -5.59 |
| 9 | 1.039 | 0.189 | 0.948 | 1.028 | 1.119 | 13.10 | -18.47 |
| 10 | 1.097 | 0.189 | 1.005 | 1.087 | 1.179 | 7.95 | -25.09 |
| 11 | 1.197 | 0.203 | 1.097 | 1.189 | 1.289 | 4.42 | -36.49 |
| 12 | 1.261 | 0.203 | 1.159 | 1.252 | 1.355 | 2.77 | -43.79 |
| 13 | 1.419 | 0.224 | 1.307 | 1.413 | 1.527 | 1.40 | -61.80 |

Note: Mean represents the average value over one million calculations. SD stands for standard deviation. Q1 refers to the first quartile, Q2 to the median, and Q3 to the third quartile. < OPC (%) indicates the proportion of carbon emissions lower than OPC in one million calculations. Compared to OPC (%) denotes the percentage reduction in average carbon emissions compared to OPC, where a positive value indicates a reduction and a negative value indicates an increase.

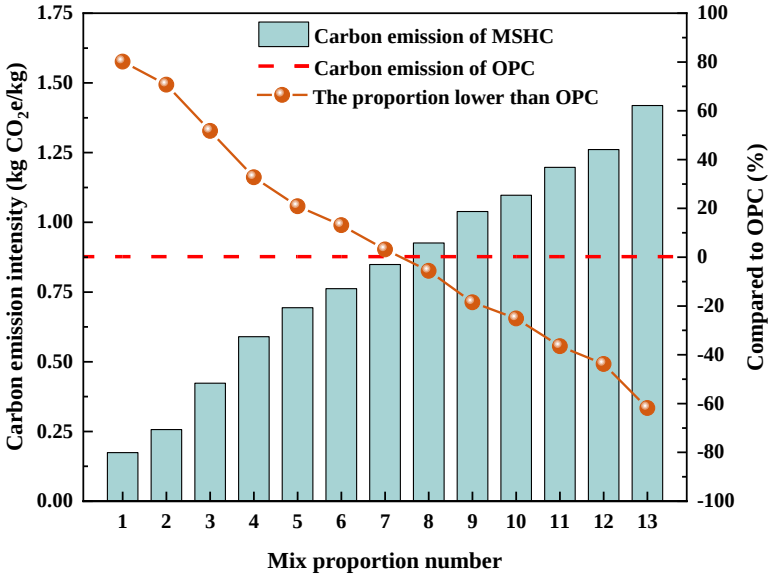


**Figure 5.** Carbon emissions of MSHC and comparison with OPC.

The calculation results indicated that, for mixing ratios 1–6, the average carbon emission intensity of MSHC ranged from a minimum of 0.174 kg $CO_2$e/kg to a maximum of 0.762 kg $CO_2$e/kg. Compared to OPC, the average carbon emission intensity of MSHC was reduced by 13.11% to 80.16%. Additionally, in the one million simulation results for these six mixing ratios, the proportion of carbon emission intensity of MSHC being lower than that of OPC exceeded 85%. This indicated that, under

these conditions, MSHC exhibited lower carbon emission intensity compared to OPC and could be considered a low-carbon material.

For mixing ratios 7 and 8, the average carbon emission intensities of MSHC were 0.849 kg $CO_2$e/kg and 0.926 kg $CO_2$e/kg, respectively, which are approximately equivalent to those of OPC. Additionally, Compared to OPC, the average change in carbon emission intensity was approximately within 5%. This indicated that, under these two mixing ratio conditions, MSHC did not demonstrate a clear advantage in terms of carbon emission intensity compared to OPC.

For mixing ratios 9–13, the average carbon emission intensities of MSHC ranged from a minimum of 1.039 kg $CO_2$e/kg to a maximum of 1.419 kg $CO_2$e/kg. These values were significantly higher than the carbon emissions of OPC. In the one million simulation results for these five mixing ratios, the highest proportion of data points with carbon emission intensity lower than that of OPC was only 13.10%. Compared to OPC, the average carbon emission intensity of MSHC was increased by 13.11% to 80.16%. This indicated that, within this range of mixing ratios, the carbon emission intensity of MSHC increased significantly, classifying it as a high carbon emission building material.

In summary, the carbon emission intensity of MSHC was closely related to its mixing ratio. Analysis of carbon emission intensity of MSHC under 13 different mixing ratios revealed that when the Mg/Si was below 0.667 (mixing ratios 1–6), MSHC exhibited significant low-carbon characteristics. However, when the Mg/Si was between 0.8 and 1.0 (mixing ratios 7–8), the carbon emission intensity of MSHC closely resembled that of OPC. Once the Mg/Si surpassed 1.0 (mixing ratios 9–13), the carbon emission intensity of MSHC increased significantly compared to OPC. It was noteworthy that these analyses did not cover all possible Mg/Si, the comparative results were considered as preliminary references. In Section 3.3, we employed a ML model to predict the relationship between changes in the Mg/Si and the carbon emissions of MSHC. Additionally, we compared the carbon emissions of MSHC and OPC under different Mg/Si.

Based on this analysis, we further summarized the carbon emission intensity results for all MSHC mix ratios in this study (a total of 13 different mix ratios, involving 13 million data points). The histogram was shown in Figure 6, and the statistical results were presented in Table 5. Our study found that the average carbon emission intensity for MSHC was 0.822 kg $CO_2$e/kg, which was 6.27% lower than that of OPC. Additionally, the proportion of MSHC's carbon emission intensity that was lower than OPC's was 54.32%. This indicated that, in a large-scale dataset, the overall carbon emission intensity of MSHC was not significantly different from that of OPC, and its environmental advantage was minimal.

However, it is worth noting that while this study emphasizes the carbon emission advantages of MSHC, it is important to acknowledge several limitations to provide a more contextualized comparison. Firstly, the current PLCA framework prioritizes carbon footprint but overlooks other critical environmental factors. For example, although MSHC utilizes industrial by-products such as silica fume and fly ash [4], whereas OPC relies on virgin limestone, the broader ecological impacts of these substitutes have not been quantified. Additionally, MSHC exhibits superior radionuclide immobilization capabilities. Through the physical encapsulation and chemical adsorption by its hydration products, MSHC can effectively immobilize radioactive strontium and cesium [7,48], but these benefits are not included in the LCA. Secondly, the differences in structural performance between the materials complicate direct comparisons. The early strength of MSHC is insufficient, limiting its application in rapid construction. However, the 28d strength of MSHC (70 MPa) [39] and its outstanding high-temperature resistance [49] make it advantageous for specialized applications, such as high-temperature industrial environments.

These limitations indicate that MSHC is not a universal substitute for OPC but rather a complementary material optimized for carbon-sensitive and extreme environments. Future life cycle assessments should incorporate multi-criteria analysis to fully capture these trade-offs.

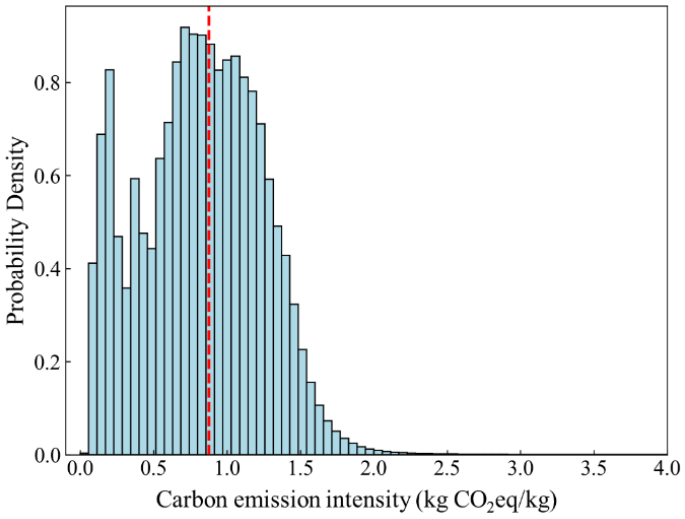


**Figure 6.** Histogram of the summary data on carbon emission intensity of MSHC.

**Table 5.** Statistical results of the summary data on carbon emission intensity of MSHC (Unit: kg $CO_2$e/kg).

| Mean | SD | Q1 | Q2 | Q3 | <OPC (%) | Compared to OPC (%) |
|---|---|---|---|---|---|---|
| 0.822 | 0.416 | 0.525 | 0.829 | 1.123 | 54.32% | 6.27 |

3.2.2. Differences and uncertainty analysis of carbon emissions among components

To further explore the uncertainty of MSHC carbon emissions, box plots were created to visually represent the carbon emissions and transportation processes for each component. It is important to note that this uncertainty analysis was conducted with fixed mixing ratios, so the primary sources of uncertainty are concentrated on the carbon emission factors of the materials. In the PLCA method, the uncertainty of input parameters is mainly propagated through Monte Carlo simulations. Specifically, each input parameter is randomly sampled to generate multiple possible values, reflecting the variability in carbon emission intensities under different production processes and raw material conditions. These values are then fed into the model to perform numerous simulation calculations, each using a different set of input parameters to mimic various real-world production scenarios. Through these multiple simulation calculations, a range of carbon emission results is obtained. These results are then statistically analyzed to generate box plots, thereby revealing the uncertainty range and key influencing factors of carbon emissions, as shown in Figure 7 (with Figure 7(a)–(m) corresponding to the results of mixing ratios 1–13, respectively).

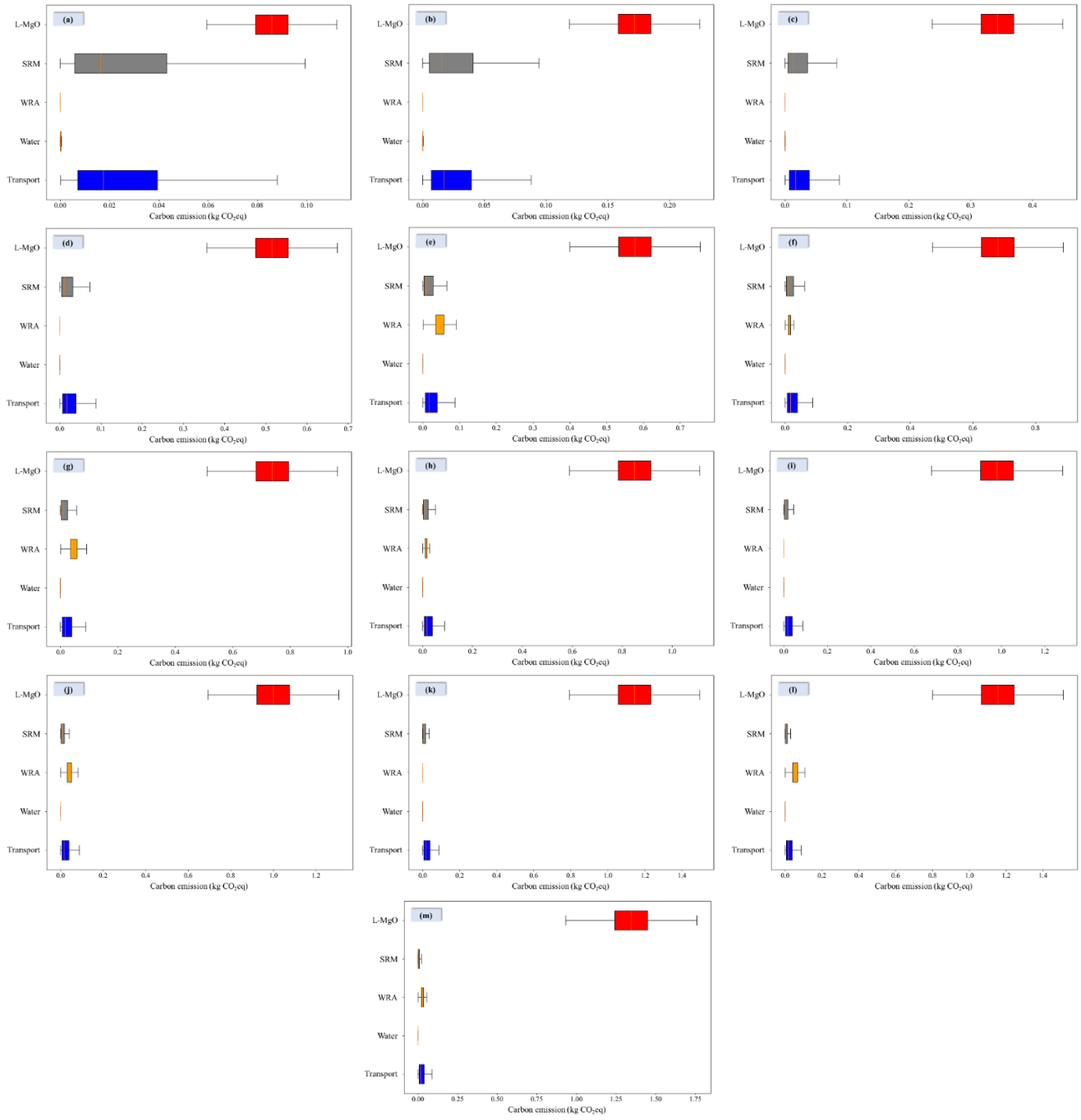


**Figure 7.** Carbon emissions from different components of MSHC at various mix proportions.

It was observed that under all mixing ratio conditions, the carbon emissions of L-MgO were the most significant, far exceeding those of other components. This indicated that L-MgO dominantly contributed to the carbon emissions of MSHC. At the same time, the carbon emissions of L-MgO also carry a significant degree of uncertainty. This uncertainty primarily stems from: Firstly, there are significant differences in production processes. Calcination temperature and duration, the type of fuel used (coal, natural gas, or renewable energy), and the handling of byproducts directly impact energy consumption and carbon emission intensity. Secondly, variations in the MgO content of the final product can lead to different amounts of $CO_2$ released during the calcination of magnesite ($MgCO_3$). Lower purity L-MgO may reduce direct carbon emissions, but it requires more raw materials and energy to

compensate for performance losses, indirectly increasing carbon intensity. In contrast, higher purity products, although they may have higher direct emissions, can enhance raw material utilization efficiency, potentially reducing the overall impact. Furthermore, the geographical heterogeneity of raw material sources (such as transportation distance, ore grade fluctuations, and differences in the energy structure of mining areas) further exacerbates the variability in carbon emissions. For instance, low-grade ores may require additional preprocessing, increasing the complexity of energy consumption and emissions. Furthermore, it was noteworthy that when the Mg/Si was low (Figure 7(a) and (b)), the carbon emissions from SRM and the transportation process also exhibited high uncertainty. This suggested that when the Mg/Si was low, attention should not only be paid to the carbon emissions of L-MgO but also to the carbon footprint of SRM and the transportation stages.

Based on the aforementioned analysis, we aggregated all data and plotted the overall box plot of carbon emissions for each component and the transportation process, as shown in Figure 8. Unlike the previous analysis with fixed mix proportions, the uncertainty in the aggregated results stems from both the material carbon emission factors and the mix design variations. Within the overall range, the carbon emissions of L-MgO remained the most prominent, with the highest uncertainty. In contrast, the carbon emissions and uncertainties of WRA, the transportation, and SRM were at moderate levels. The carbon emissions and uncertainties of water were the lowest. This result further confirms that L-MgO was the primary factor in MSHC carbon emissions. This was attributed to the higher usage and the carbon-intensive production process of L-MgO. Therefore, optimizing the production processes and sources of L-MgO specifically would be a key approach to reducing MSHC carbon emissions.

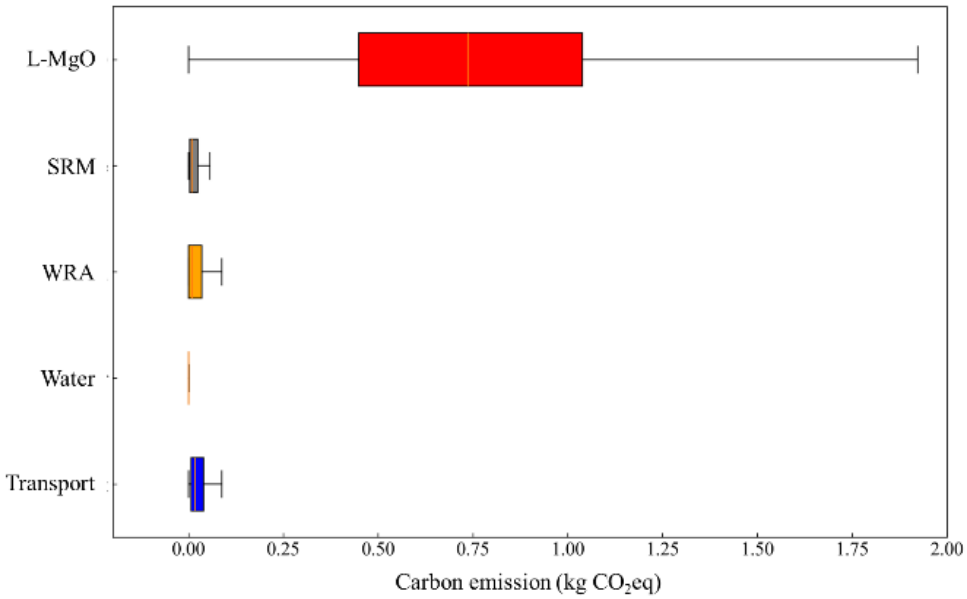


**Figure 8.** Carbon emissions from different components of MSHC after data aggregation.

3.2.3. Design of GUI for carbon emission of MSHC based on PLCA

To enhance the convenience of analytical tools, this study developed a GUI based on the PLCA method for calculating the carbon emission intensity of MSHC, as shown in Figure 9. Figure 9 illustrates the operational process of this GUI and its output results. First, users input relevant parameters in the designated input fields, including the mix proportions of MSHC, transportation distance, and the number

of simulations. These input parameters directly affect the carbon emission outcomes during the simulation process. Upon clicking the simulate button, the system performs multiple simulation calculations based on the entered parameters, reflecting various possible carbon emission scenarios through random sampling and model propagation. Ultimately, the system generates a series of carbon emission intensity results and visualizes them using probability density plots and statistical characteristics. The design of this GUI is simple and intuitive, allowing users without specialized programming or data analysis skills to easily conduct carbon emission simulations and analyses. It provides an efficient and convenient tool for analyzing the carbon emissions of MSHC. This GUI is suitable for researchers who require extensive data analysis and model validation. By using the PLCA-based GUI, researchers can quickly perform multiple simulations to obtain carbon emission distributions and statistical characteristics under different conditions. This is crucial for gaining a deeper understanding of the carbon emission mechanisms of MSHC and optimizing its mix design. Furthermore, given that the PLCA method involves complex probabilistic calculations, this tool helps researchers save considerable time and effort, thereby improving research efficiency.

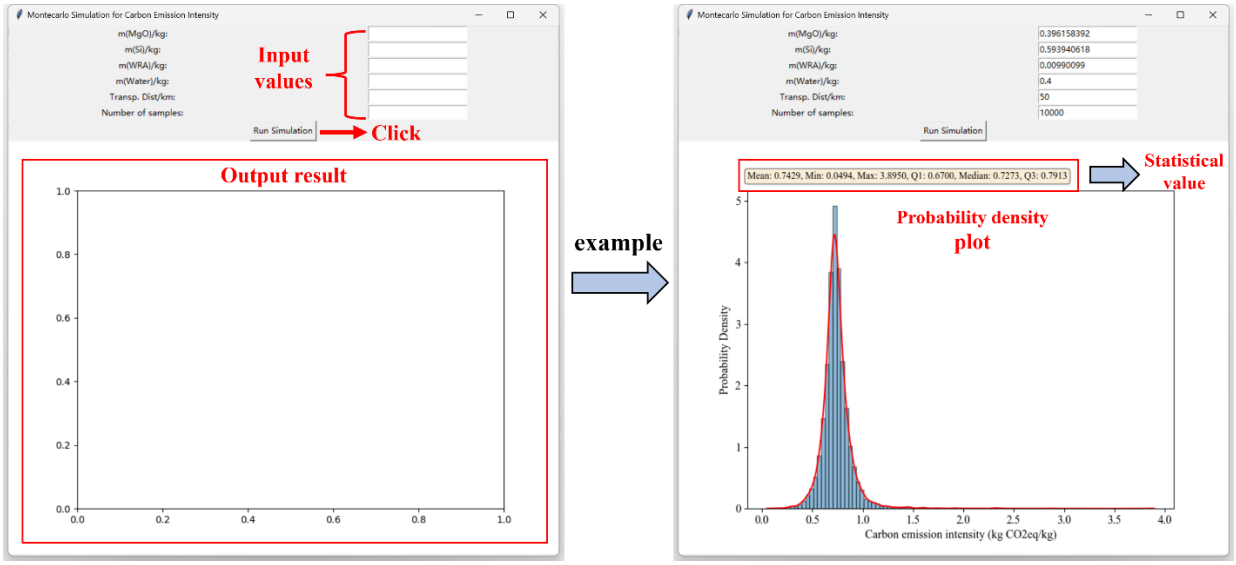


**Figure 9.** GUI design for the carbon emissions of MSHC based on PLCA.

### *3.3. Construction and analysis of the carbon emission prediction model*

#### 3.3.1. Establishment of ML models

To enhance the prediction of carbon emission intensity for various MSHC ratios, a ML method was utilized to develop a predictive model for MSHC carbon emissions. A total of 650,000 data points were randomly sampled from the simulation data, forming a dataset with 10 input variables. The input variables consisted of the carbon emission factors for raw materials and diesel (c(L-MgO), c(SRM), c(WRA), c(Water), c(Diesel)), the usage quantities of raw materials (m(L-MgO), m(SRM), m(WRA), m(Water)), and the transportation distance (Dis). The output target was the carbon emission intensity of MSHC, measured in kg$CO_2$e.

During the machine learning modeling process, 70% of the data was set aside as the training set, while 30% was used as the test set. The predictive performance of each model is shown in Table 6. As seen from

the table, the $R^2$ values for all models exceeded 0.95, indicating a high level of predictability within the dataset used in this study. Among the different models, the RF model achieved an $R^2$ value of 0.999 for the training data and 0.993 for the test data. Furthermore, it demonstrated the lowest error values. These findings indicate that the RF model excelled in predicting the carbon emission intensity of MSHC.

**Table 6.** Predictive performance metrics for ML models.

| Indicators | Data set | Models | | | |
|---|---|---|---|---|---|
| | | LR | DT | XGB | RF |
| $R^2$ | train | 0.965 | 0.998 | 0.998 | 0.999 |
| | test | 0.965 | 0.985 | 0.991 | 0.993 |
| MAE | train | $4.19 \times 10^{-2}$ | $1.21 \times 10^{-2}$ | $5.52 \times 10^{-3}$ | $5.01 \times 10^{-3}$ |
| | test | $4.13 \times 10^{-2}$ | $2.51 \times 10^{-2}$ | $1.21 \times 10^{-2}$ | $1.03 \times 10^{-2}$ |

To improve the practicality of the ML model and meet the requirements of practical applications, a GUI was developed for predicting the carbon emission intensity of MSHC using the RF model, as shown in Figure 10. Unlike the previous GUI designed based on PLCA, this GUI required users to input deterministic data, including the MSHC mix ratio, carbon emission factors of each component and diesel, and transportation distance. It did not use randomly generated data. This allowed users to quickly obtain MSHC carbon emission results for different MSHC ratios and carbon emission factors that align with their actual production scenarios. This GUI is primarily aimed at industry professionals and practical application scenarios. In actual production processes, professionals need to quickly and accurately predict carbon emissions for decision-making and optimization of production processes. Compared to traditional methods, the ML-based GUI offers a simple and efficient solution, allowing users to input specific production data and immediately obtain carbon emission predictions. This not only improves work efficiency but also ensures the practicality and reliability of the prediction results. It is of great significance for promoting low-carbon production and optimizing management.

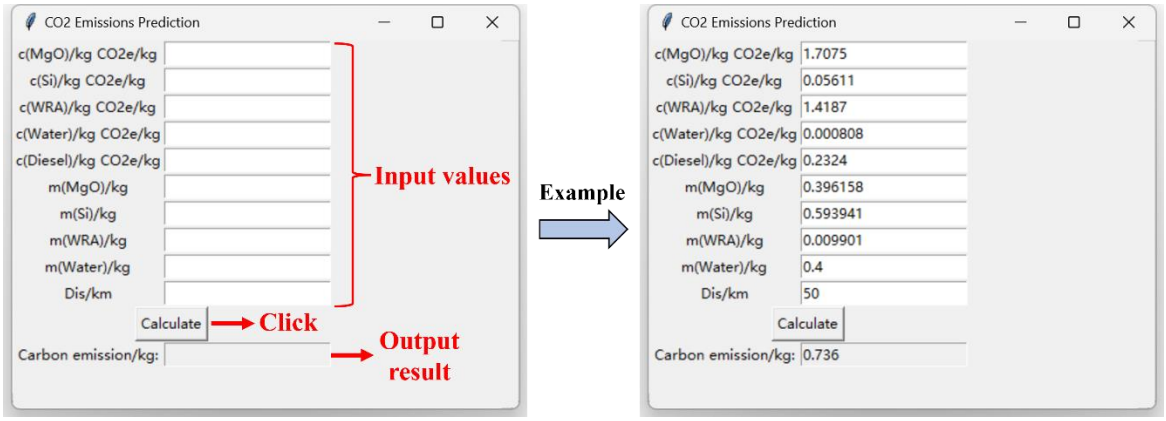


**Figure 10.** GUI design for the carbon emissions of MSHC based on machine learning.

3.3.2. Feature importance analysis

The previous section indicated that the RF model performed best in predicting carbon emissions of MSHC. Consequently, SHAP analysis was performed using the RF calculation results to examine the

influence of each input parameter on the output parameter. Figure 11 presented the average SHAP values for each input parameter, reflecting their respective influence on the output results. The larger the average SHAP value, the more significant its impact on the output results.

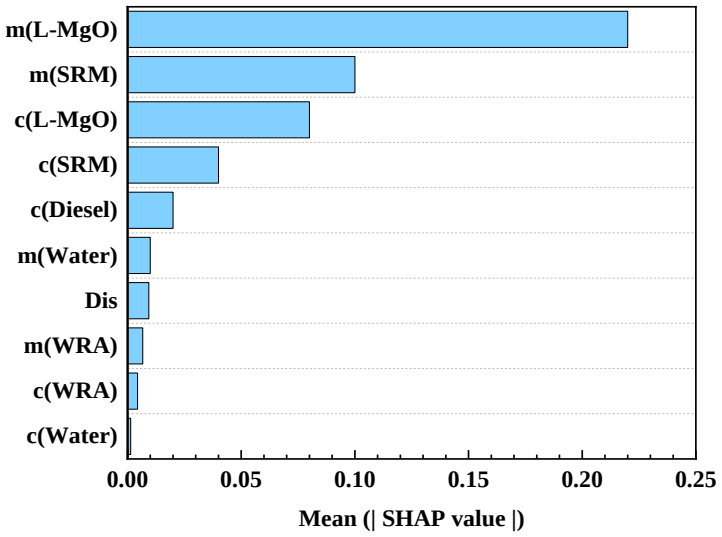


**Figure 11.** Feature importance analysis.

The results indicated that among all features, m(L-MgO) and m(SRM) had a significant impact on the carbon emissions of MSHC, reflecting the critical role of the Mg/Si ratio. This was consistent with the aforementioned analysis. Following these, c(L-MgO), c(SRM), and c(Diesel) also exhibited considerable influence. Additionally, m(Water) and Dis showed a certain degree of impact on the carbon emissions of MSHC. In contrast, m(WRA), c(WRA), and c(Water) had relatively minor effects.

In summary, the Mg/Si ratio has been identified as a core factor in the MSHC carbon footprint, and optimizing and lowering the Mg/Si ratio is a key measure for reducing carbon emissions. Furthermore, to further promote material decarbonization, industrial waste was considered as a partial replacement for L-MgO, such as using industrial by-products or waste containing magnesium as alternative raw materials [50]. This approach not only helps reduce dependence on virgin resources but also effectively lowers carbon emissions during production. Additionally, further optimizing the carbon emissions in the production processes of L-MgO and SRM, reducing water consumption, and improving transportation efficiency are all critical measures for making MSHC production more environmentally friendly. Therefore, by implementing comprehensive measures for efficient resource utilization and emission reduction, significant progress can be made toward green MSHC production. This provides important support for building a low-carbon circular economy within the construction materials industry.

### 3.3.3. Analysis of the impact of key factors

Mg/Si was identified as a core factor influencing MSHC carbon emissions. To further quantify the impact of Mg/Si on MSHC carbon emissions, an RF model was used to predict the carbon emission intensity of MSHC across 390 different mixing ratios with Mg/Si ranging from 0.1 to 4.0, at 0.01 intervals. The study results were illustrated in Figure 12, where the red line indicated the reference value for OPC carbon emissions. The carbon emission factor was chosen as the average, median, and the first and third quartiles of the carbon emission factors for each component.

As illustrated in Figure 12, the carbon emissions of MSHC progressively increased with the rise in the Mg/Si ratio. Specifically, when using the first quartile as the carbon emission factor, the carbon emission intensity of MSHC matched that of OPC at an Mg/Si ratio of approximately 1.25. When the mean and median values were used as the carbon emission factors, the equivalence point occurred around an Mg/Si ratio of 1.0. With the third quartile value set as the carbon emission factor, the equivalence point shifted to approximately 0.85.

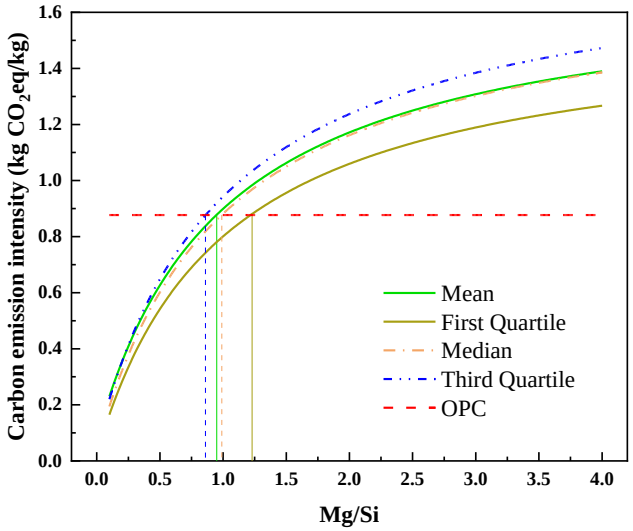


**Figure 12.** The relationship between Mg/Si and the carbon emission of MSHC.

In summary, under different carbon emission factor settings, when the Mg/Si ratio is between 0.85 and 1.25, the carbon emission intensity of MSHC is essentially consistent with that of OPC. However, when the Mg/Si ratio exceeds this range, MSHC ceases to be a low-carbon material and may even transition into a high-carbon building material. Therefore, controlling the Mg/Si ratio within an appropriate range is crucial for achieving low carbon emissions.

## 4. Conclusion

In this study, a PLCA method was used to conduct a quantitative evaluation and uncertainty analysis of carbon emissions of MSHC. On this basis, ML was utilized to create a predictive model for the carbon emission intensity of MSHC, followed by a sensitivity analysis on the key parameters. Additionally, two GUI based on PLCA and ML were developed for rapid analysis and prediction of carbon emissions of MSHC. The study demonstrated that:

- Based on different mix proportions, the simulated carbon emission intensity of MSHC ranged from 1.40% to 98.98% lower than that of OPC. This indicated that MSHC was not definitively a low-carbon cementitious material, as its carbon emissions were highly dependent on its mix proportion adjustments.
- Due to the high carbon emission factor and substantial usage of L-MgO, it dominated the overall carbon emissions of MSHC and was the key factor influencing the uncertainty in carbon emissions of MSHC.
- Feature importance analysis indicated that m(L-MgO) and m(SRM) (Mg/Si ratio) had the most significant impact on the carbon emissions of MSHC, followed by factors such as c(L-MgO), c(SRM), and c(Diesel).

- A threshold effect was observed for the Mg/Si: when the Mg/Si is below approximately 0.8, MSHC exhibits notable low-carbon characteristics. However, when the Mg/Si exceeds approximately 1.0, the carbon emission intensity of MSHC does not demonstrate a clear advantage and may even become a high-carbon building material.

## Acknowledgments

The authors would like to acknowledge the financial support of Chongqing Natural Science Foundation (No.CSTB2022NSCQ-MSX1250) and the National Key Research and Development Program (No.2022YFC3803103).

## Data availability

The data from this study can be obtained from the corresponding author upon reasonable request.

## Authors' contribution

Yue Li: methodology, investigation, resources, supervision, project administration, funding acquisition, writing—review and editing. Xiao Luo: conceptualization, methodology, software, validation, formal analysis, investigation, data curation, writing—original draft preparation. Xiaolong Liu: investigation, data curation, software, visualization. Zhijie Zhang: methodology, software, validation. Kun Meng: methodology, software, data curation. Jinlei Mu: software, investigation, conceptualization.

## Conflicts of interests

The authors declare no conflict of interest.

## References

[1] Izumi Y, Iizuka A, Ho H. Calculation of greenhouse gas emissions for a carbon recycling system using mineral carbon capture and utilization technology in the cement industry. *J. Cleaner Prod.* 2021, 312:127618.

[2] Ali MB, Saidur R, Hossain MS. A review on emission analysis in cement industries. *Renewable Sustainable Energy Rev.* 2011, 15(5):2252–2261.

[3] Hasanbeigi A, Price L, Lin E. Emerging energy-efficiency and $CO_2$ emission-reduction technologies for cement and concrete production: a technical review. *Renewable Sustainable Energy Rev.* 2012, 16(8): 6220–6238.

[4] Sreenivasan H, Bernard E, Santos HS, Nguyen H, Moukannaa S, *et al.* A critical review of magnesium silicate hydrate (M-S-H) phases for binder applications. *Cem. Concr. Res.* 2024, 178:107462.

[5] Jin F, Al-Tabbaa A. Strength and hydration products of reactive MgO-silica pastes. *Cem. Concr. Compos.* 2014, 52:27–33.

[6] Tran HM, Scott A. Strength and workability of magnesium silicate hydrate binder systems. *Constr. Build. Mater.* 2017, 131:526–535.

[7] Zhang T, Zou J, Li Y, Jia Y, Cheeseman CR. Stabilization/solidification of strontium using magnesium silicate hydrate cement. *Processes* 2020, 8(2):163.

[8] Ruan S, Unluer C. Comparative life cycle assessment of reactive MgO and Portland cement production. *J. Cleaner Prod.* 2016, 137:258–273.

[9] Zhang T, Li T, Zhou Z, Li M, Jia Y, Cheeseman CR. A novel magnesium hydroxide sulfate hydrate whisker-reinforced magnesium silicate hydrate composites. *Composites, Part B* 2020, 198:108203.

[10] Zheng K, Xie X, Gou G, Chen X, Huang Y, *et al.* Comparative study on characteristics and microstructure of magnesium silicate hydrate utilizing quartz and silica fume as siliceous raw materials. *Case Stud. Constr. Mater.* 2023, 19:e2313.

[11] Li Y, Luo X, Lin H, Li H, Liu Y, *et al.* The impact of environmental humidity on the mechanical property and microstructure of magnesium silicate hydrate cement. *Constr. Build. Mater.* 2024, 425:135966.

[12] Ige OE, Olanrewaju OA, Duffy KJ, Obiora C. A review of the effectiveness of life cycle assessment for gauging environmental impacts from cement production. *J. Cleaner Prod.* 2021, 324:129213.

[13] Mendoza Beltran A, Prado V, Font Vivanco D, Henriksson PJG, Guinée JB, *et al.* Quantified uncertainties in comparative life cycle assessment: what can be concluded? *Environ. Sci. Technol.* 2018, 52(4):2152–2161.

[14] O'Brien KR, Ménaché J, O'Moore LM. Impact of fly ash content and fly ash transportation distance on embodied greenhouse gas emissions and water consumption in concrete. *Int. J. Life. Cycle. Assess.* 2009, 14(7):621–629.

[15] Xing W, Tam VW, Le KN, Hao J, Wang J. Life cycle assessment of sustainable concrete with recycled aggregate and supplementary cementitious materials. *Resour. Conserv. Recycl.* 2023, 193:106947.

[16] Al-Fakih A, Al-wajih E, Saleh RAA, Muhit IB. Ensemble machine learning models for predicting the $CO_2$ footprint of GGBFS-based geopolymer concrete. *J. Cleaner Prod.* 2024, 472:143463.

[17] Wang S, Chen K, Liu J, Xia P, Xu L, *et al.* Multi-performance optimization of low-carbon geopolymer considering mechanical, cost, and $CO_2$ emission based on experiment and interpretable learning. *Constr. Build. Mater.* 2024, 425:136013.

[18] Thilakarathna PSM, Seo S, Baduge KSK, Lee H, Mendis P, *et al.* Embodied carbon analysis and benchmarking emissions of high and ultra-high strength concrete using machine learning algorithms. *J. Cleaner Prod.* 2020, 262:121281.

[19] Li Z, Zhang T, Hu J, Tang Y, Niu Y, *et al.* Characterization of reaction products and reaction process of MgO-$SiO_2$-$H_2O$ system at room temperature. *Constr. Build. Mater.* 2014, 61:252–259.

[20] Li J, Zhang Y, Shao S, Zhang S. Comparative life cycle assessment of conventional and new fused magnesia production. *J. Cleaner Prod.* 2015, 91:170–179.

[21] P. Li, B. Chen, Q. Cui. A probabilistic life-cycle assessment of carbon emission from magnesium phosphate cementitious material with uncertainty analysis. *J. Cleaner Prod.* 2023, 427: 139164.

[22] Shen W, Cao L, Li Q, Wen Z, Wang J, *et al.* Is magnesia cement low carbon? Life cycle carbon footprint comparing with Portland cement. *J. Cleaner Prod.* 2016, 131:20–27.

[23] China Products Carbon Footprint Factors Database. Available: https://lca.cityghg.com. (accessed on 25 February 2025).

[24] Ma F, Sha A, Yang P, Huang Y. The greenhouse gas emission from Portland cement concrete pavement construction in China. *Int. J. Environ. Res. Public Health.* 2016, 13(7):632.

[25] Gunasekara C, Sandanayake M, Zhou Z, Law DW, Setunge S. Effect of nano-silica addition into high volume fly ash–hydrated lime blended concrete. *Constr. Build. Mater.* 2020, 253:119205.

[26] Alnahhal MF, Alengaram UJ, Jumaat MZ, Abutaha F, Alqedra MA, *et al.* Assessment on engineering properties and $CO_2$ emissions of recycled aggregate concrete incorporating waste products as supplements to Portland cement. *J. Cleaner Prod.* 2018, 203:822–835.

[27] Chen C, Habert G, Bouzidi Y, Jullien A, Ventura A. LCA allocation procedure used as an incitative method for waste recycling: an application to mineral additions in concrete. *Resour. Conserv. Recycl.* 2010, 54(12):1231–1240.

[28] Sonat C, Kumar D, Koh WC, Li J, Unluer C, *et al.* Strain hardening magnesium-silicate-hydrate composites with extremely low fiber dosage of 0.5% by volume. *Cem. Concr. Compos.* 2023, 142:105200.

[29] Miller SA. Supplementary cementitious materials to mitigate greenhouse gas emissions from concrete: can there be too much of a good thing? *J. Cleaner Prod.* 2018, 178:587–598.

[30] Schiefer C, Plank J. $CO_2$ emission of polycarboxylate superplasticizers (PCEs) used in concrete. *J. Cleaner Prod.* 2023, 427:138785.

[31] Moghadam AS, Omidinasab F, Goodarzi SM. Characterization of concrete containing RCA and GGBFS: Mechanical, microstructural and environmental properties. *Constr. Build. Mater.* 2021, 289:123134.

[32] Purnell P, Black L. Embodied carbon dioxide in concrete: variation with common mix design parameters. *Cem. Concr. Res.* 2012, 42(6): 874–877.

[33] Kim JE, Seo J, Yang K, Kim HK. Cost and $CO_2$ emission of concrete incorporating pretreated coal bottom ash as fine aggregate: a case study. *Constr. Build. Mater.* 2023, 408:133706.

[34] Robati M, McCarthy TJ, Kokogiannakis G. Incorporating environmental evaluation and thermal properties of concrete mix designs. *Constr. Build. Mater.* 2016, 128:422–435.

[35] Hong J, Shen GQ, Peng Y, Feng Y, Mao C. Uncertainty analysis for measuring greenhouse gas emissions in the building construction phase: a case study in China. *J. Cleaner Prod.* 2016, 129: 183–195.

[36] Luo X, Li Y, Lin H, Li H, Shen J, *et al.* Effect of curing regimes on strength of magnesium silicate hydrate cement. *J. Mater. Res. Technol.* 2023, 26:7534–7546.

[37] Luo X, Li Y, Lin H, Li H, Shen J, *et al.* Research on predicting compressive strength of magnesium silicate hydrate cement based on machine learning. *Constr. Build. Mater.* 2023, 406:133412.

[38] Eubank WR. Calcination Studies of Magnesium Oxides. *J. Am. Ceram. Soc.* 1951, 34:225–229.

[39] Zhang T, Vandeperre LJ, Cheeseman CR. Formation of magnesium silicate hydrate (M-S-H) cement pastes using sodium hexametaphosphate. *Cem. Concr. Res.* 2014, 65:8–14.

[40] Jin F, Gu K, Al-Tabbaa A. Strength and hydration properties of reactive MgO-activated ground granulated blastfurnace slag paste. *Cem. Concr. Compos.* 2015, 57:8–16.

[41] Kumar S, Sonat C, Yang E, Unluer C. Performance of reactive magnesia cement formulations containing fly ash and ground granulated blast-furnace slag. *Constr. Build. Mater.* 2020, 232:117275.

[42] Taj K, Akturk B, Ulukaya S. Fresh state properties and compressive strength development of reactive MgO-based systems. *Mater. Today: Proc.* 2022, 65:1064–1069.

[43] Mármol G, Savastano H, Tashima MM, Provis JL. Optimization of the MgO $SiO_2$ binding system for fiber-cement production with cellulosic reinforcing elements. *Mater. Des.* 2016, 105:251–261.

[44] Cao Z, Shen L, Zhao J, Liu L, Zhong S, *et al.* Toward a better practice for estimating the $CO_2$ emission factors of cement production: An experience from China. *J. Cleaner Prod.* 2016, 139:527–539.

[45] Yu X, Tan C. China's process-related greenhouse gas emission dataset 1990–2020. *Sci. Data.* 2023, 10(1):55–59.

[46] Luo X, Li Y, Wang Q, Mu J, Liu Y. Machine learning based modeling for predicting the compressive strength of solid waste material-incorporated magnesium phosphate cement. *J. Cleaner Prod.* 2024, 442:141172.

[47] Zhu X, Zhang Y, Liu Z, Qiao H, Ye F, *et al.* Research on carbon emission reduction of manufactured sand concrete based on compressive strength. *Constr. Build. Mater.* 2023, 403:133101.

[48] Zhang T, Li T, Zou J, Li Y, Zhi S, *et al.* Immobilization of radionuclide 133Cs by magnesium silicate hydrate cement. *Mater.* 2020, 13(1):146.

[49] Ma H, Zhang S, Feng J. Physicochemical properties of MgO-silica fume cementitious materials exposed to high temperatures. *J. Build. Eng.* 2022, 50:104124.

[50] Zhang Z, Hua Y, Wen J, Li Z, Qian J. Preparation and properties of magnesium silicate cement with magnesium slag extracted lithium from salt lake. *Constr. Build. Mater.* 2025, 471:140750.